ISSN 1330-3651 (Print), ISSN 1848-6339 (Online) https://doi.org/10.17559/TV-20220321024747
Original scientific papers

Numerical Investigation of Evolution Characteristics of Ultrafine Tailings Backfill Slurry Flow Considering Slurry Temperature

Deqing GAN, Haikuan SUN*, Yajie ZHANG, Zhenlin XUE

Abstract: To analyze the effect of slurry temperature on Ultrafine tailings backfill slurry (UTBS) flow characteristics, a new comprehensive Reynolds number (R_c) model considering slurry temperature for determining the flow pattern of UTBS was proposed. The flow evolution characteristics of UTBS considering the effect of slurry temperature were investigated under the condition of coupled multi-physical fields. UTBS flow velocity field was divided into shear zone and structural flow zone. With the flow proceeded, the area of the structural flow zone decreased. Increasing slurry temperature could generate more gel, which could wrap the tailings particles and reduce the resistance loss. When transport flow increased, the interaction between UTBS particles and friction increased, which caused the resistance loss to increase. Influenced by "non-uniform interference settlement" and the law of tailing sand particle transport, the resistance loss increased with the increase of stowing gradient. This paper suggests that the mine could choose a transport flow rate of 220 m^3/h and stowing gradient of 5 as a reference for pipeline transport.

Keywords: comprehensive Reynolds number; flow evolution characteristics; numerical investigation; slurry temperature; ultrafine tailings backfill slurry

1 INTRODUCTION

Pipeline transportation is a key component to ensure that the backfill slurry is transported to the stope. With the increase in plastic viscosity, yield stress leads to an enlarged viscous resistance between the slurry flow layers and a decrease in the average speed of transport, which seriously affects the efficiency of transportation [1-3]. The resistance loss is affected by many factors such as pipe diameter, initial velocity and cement-sand ratio. Researchers have conducted large-diameter slurry transport experiments, and optimized the cement-sand ratio, flow velocity and resistance loss for high-flow slurry transport to achieve mining and filling coordination [4]. The variation of cemented slurry wall slip for different pipe diameters has been studied with volume concentration, particle size and slurry temperature as variables [5]. Besides, the size of the tailings particles affects the pressure drop and concentration distribution in the pipeline. For example, coarser particles move on the slip bed in the low velocity zone, which indicates that the size of the tailing's particles has an effect on the flow characteristics of the slurry pipeline transportation [6]. In addition, Alireza investigated the effect of physical parameters such as valve closing time, length of measurement time and noise level on the location of the most common blockages in pipeline transportation and analyzed the existence of trade-offs between the degree, location and length of blockage [7]. Meanwhile, the type of backfill material also has influence on the resistance loss [8].

Due to the continuous development of mineral resources, the remaining number of easy-to-elect ore has been gradually decreasing. Therefore, deep grinding of difficult-to-elect ore is necessary in mineral processing to extract useful minerals, which leads to the decreasing size of tailings and the increasing proportion of ultrafine tailings [9, 10]. Ultrafine tailings are customarily referred to as $d_{80} \leq 20$ μm tailings. Both conventionally sized backfill slurry and UTBS are Bingham plastic fluids with time-temperature dependence [11]. In slurry transportation, heat is generated by the collision between solid phase particles, friction between particles and pipe wall, and hydration. In addition, the ambient temperature gradually increases as the depth of the mine increases. These factors lead to an increase in slurry temperature and changes in rheological parameters and pipeline flow characteristics. Therefore, the influence on slurry temperature cannot be neglected [12, 13]. Studies have proved that the rheological properties of concrete, natural water-lime slurry and slag slurry are changed by temperature change [14, 15]. In addition, variations in slurry temperature change the comprehensive Reynolds number (R_c), which has an impact on the flow pattern of UTBS. Failure to consider the effect of slurry temperature when designing pipeline transport parameters can lead to clogging and pipe bursting accidents. Using the annular pipe experiment for slurry flow characteristics exploration has the disadvantages of high cost and poor operability. Numerical simulation could solve this problem better and obtain more reliable experiment data. However, there is a slight lack of relevant studies and reports in this area.

This paper innovatively explored the flow evolution characteristics of UTBS under the influence of slurry temperature. A comprehensive Reynolds number model considering the effect of slurry temperature was developed to discriminate the flow pattern. A coupled multi-physics field model of UTBS flow was constructed to investigate the effects of slurry temperature, transport flow and stowing gradient on the velocity field and resistance loss of UTBS flow process. The reliability of the model was verified. The particle transport mechanism of UTBS was described. The conclusions could provide some guidance basis in the design of backfill pipeline and establish the theoretical basis for future physical tests of pipeline transportation.

2 MODELS AND METHODS

2.1 Mathematical Model

Slurry flow model conforms to Bingham plastic fluid [16]. The rheological parameters are calculated by the following equation:

$$\tau=\tau_0+\eta_0\cdot\frac{\mathrm{d}u}{dy} \tag{1}$$

where, τ is the shear stress; τ_0 is the initial shear stress; η_0 is the plastic viscosity; du/dy is the shear rate.

Based on the Newtonian fluid resistance loss expression, the R_c equation used to calculate the evolution of the slurry flow pattern can be derived:

$$i=\frac{64}{\frac{\rho Dv}{\eta_0}}\left(1+\frac{\tau_0 D}{6\eta_0 v}\right)\frac{v^2}{2gD} \tag{2}$$

$$R_c=\frac{\rho vD}{\eta_0\left(1+\frac{\tau_0 D}{6\eta_0 v}\right)} \tag{3}$$

where D is the pipe diameter, ρ is the slurry density, and R_c is the comprehensive Reynolds number.

When the R_c is greater than 2000, the flow pattern is turbulent. Conversely, it is laminar flow (see Fig. 1) [17].

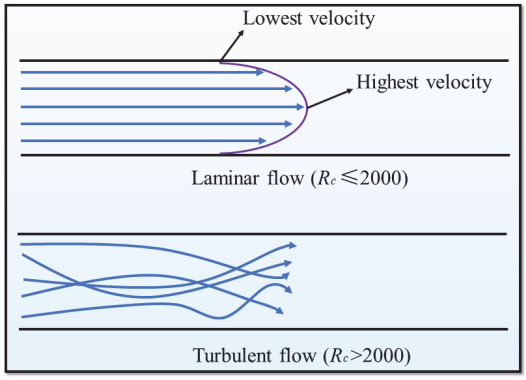

Figure 1 Schematic diagram of slurry flow pattern

The heat transfer phenomenon of slurry during pipeline transportation can be explained by the fluid heat transfer equation [18]:

$$\begin{aligned}&\rho C_P u\nabla T+\nabla\cdot q=Q+Q_P+Q_{vd}\\&q=-k\nabla T\end{aligned} \tag{4}$$

where, u is the slurry flow velocity; C_p is the heat capacity of slurry; ∇T is the temperature gradient; Q is the heat source in the flow process (including hydration heat release, etc.); Q_p is pressure acting heat transfer; Q_{vd} is heat generated by other actions, q is heat transfer rate; $\nabla\cdot q$ is the heat rate divergence.

Slurry temperature affects the heat production of hydration through the rate of hydration reaction, and the model for calculating the quantity of heat of hydration is as follows [19]:

$$Q_w=Q_0-A\exp\left(-k\sum_{i=1}^{n}\left(\frac{k_t}{k}\right)\Delta\tau_i\right) \tag{5}$$

where, Q_w is heat release during hydration; Q_0 is the final heat generation of cement mineral; k_t is the reaction rate at room temperature; k is the reaction rate at temperature; τ_i is equivalent time; A is the constant.

Gravity transportation is a method of transporting slurry without relying on external forces only by using the gravitational potential energy of the vertical height difference to overcome the resistance of the horizontal pipe in the transportation process [20].

Stowing gradient is a critical factor affecting gravity transportation. The calculation model N_m for max allowable stowing gradient of UTBS conveying is expressed as:

$$N_m=\frac{\rho g}{1.3}\cdot\frac{1}{\frac{16\tau_0}{3D}+\frac{32\eta v}{D^2}} \tag{6}$$

where, g is gravity acceleration.

2.2 Governing Equation

(1) Laminar flow.

When the slurry flow state is laminar flow, the flow process follows to laminar energy equation, momentum equation, continuity equation and particle motion state equation [21, 22].

(2) Turbulent flow.

When the slurry flow is a relatively complex turbulent flow, the k-ε turbulence model is generally chosen to describe it. The flow process in a circular pipe follows the turbulent continuity equation, momentum equation and energy equation [23, 24].

2.3 Model Parameters

The experiment parameters were set as follows: Flow gradients were 180 m³/h, 200 m³/h, 220 m³/h, 240 m³/h and 260 m³/h, and pipe diameter was 200 mm. Temperature was set at 30 ℃, 40 ℃, 50 ℃ and 60 ℃, stowing gradient was 3, 5 and 7, and slurry density was 1850 kg/m³.

The following assumptions were made in the flow process: (1) UTBS was regarded as incompressible fluid in the simulation process. (2) When UTBS was stationary or flowing in the pipe, there was no gap. (3) The flow process satisfied the normal steady flow, and the anisotropic mechanical characteristics were consistent.

2.4 Model Verification

The reliability of the model can be verified by comparing the resistance loss values recorded in the simulation with the measured. Tab. 1 provides the parameters of mine pipeline transportation.

Table 1 Verification experimental parameters

Experimental parameters	Different pipe diameters	Different transport flows
Transport flow / m³/h	70	40, 50, 60, 70, 80
Slurry density / kg/m³	1820	1820
Pipe diameter / mm	120, 130, 140, 150, 160	140
Plastic viscosity / Pa·s	20,2	20,2
Stowing gradient	3	3

The verification and comparison of simulated and measured resistance loss are shown in Fig. 2. Fig. 2 shows that when the transport flow and pipe diameter are respectively variable, the measured and simulated

resistance loss error is 2.15% and 4.50%. It indicates that the model has a reliable simulation effect.

The convergence of the simulation results is an important criterion to test whether the model is reasonable. The relative tolerance is set as 10^{-5} in the experiment, and the convergence diagram after the simulation is analyzed. When the calculated error is less than the relative tolerance after a certain number of iterations, the calculated value is considered to satisfy the condition and is true. Fig. 3 represents the convergence graph of the computational results.

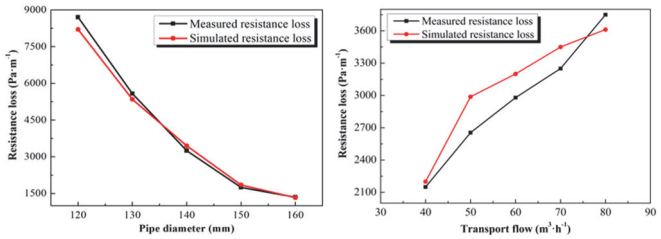

(a) Different pipe diameter (b) Different transport flow

Figure 2 Verification of resistance loss

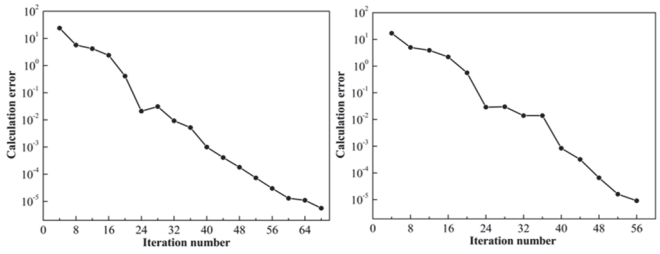

(a) Different pipe diameter (b) Different transport flow

Figure 3 Convergence curve of simulation results

In Fig. 3a, it is less than the relative tolerance after 68 computational iterations with an error of 5.6×10^{-6}. In Fig. 3b, it is less than the relative tolerance of 10^{-5} after 56 computational iterations with an error of 9.1×10^{-6}. It shows that the simulation results are converged and the model is reasonable and feasible.

3 RESULTS AND DISCUSSION

3.1 Comprehensive Reynolds Number Model

Yield stress and plastic viscosity of slurry are affected by the change of slurry temperature. To explore the relationship between the slurry temperature and the R_c, the influence of slurry temperature on yield stress and plastic viscosity should be discussed.

Rheological experiments were conducted using HAKKES series rheometers to obtain the rheological properties of shear stress and shear rate curves. Then, the plastic viscosity and yield stress of UTBS were analyzed at different slurry temperatures.Tab. 2 shows the slurry temperature relationship with rheological parameters.

Table 2 Rheological parameters under different slurry temperatures

Slurry temperature / °C	Plastic viscosity / Pa·s	Yield stress / Pa
30	0,62	225,10
40	0,57	200,55
50	0,53	181,47
60	0,51	159,72

Based on the above data, origin mapping software was used to fit the relation curve between slurry temperature, plastic viscosity and yield stress, as shown in Fig. 4.

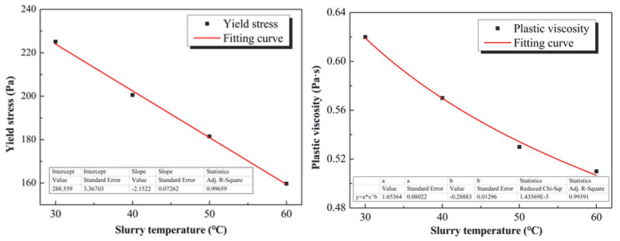

(a) Plastic viscosity (b) Yield stress

Figure 4 Fitting curse between slurry temperature and rheological parameters

The relationship between slurry temperature, plastic viscosity and yield stress is as follows:

$$\eta_0 = 1.654T^{-0.289} \qquad R^2 = 0.994 \tag{7}$$

$$\tau_0 = -2.152T + 288.56 \qquad R^2 = 0.997 \tag{8}$$

By combining Eq. (3), Eq. (7) and Eq. (8), the relationship between slurry temperature and R_c can be obtained:

$$R_c = \frac{\rho v D}{1.654T^{-0.289}\left(1+\dfrac{(-2.152T+288.56)D}{9.924T^{-0.289}v}\right)} \tag{9}$$

Eq. (9) is used to calculate the R_c of different flow velocity and slurry temperature. Tab. 3 shows the corresponding relationship between transport flow and initial velocity. The results of R_c calculation are shown in Tab. 4.

Tab. 4 indicates that the R_c of each group is far less than 2000. Therefore, the flow pattern of UTBS is stable under the test conditions and the flow process is laminar. Consequently, in this simulation experiment, selecting the laminar flow model and the governing equations in the laminar flow condition is reasonable.

With the slurry temperature increasing, the plastic viscosity and yield stress decrease. With the shear between the slurry decreasing, the viscosity between the flow layers reduces, which results in an increase in the flow velocity of the UTBS and a decrease in flow stability, therefore, the R_c increases. When the transport flow increases, the flow velocity of the UTBS from the vertical pipe into the horizontal pipe would increase. This leads to increased collision between particles, enhanced frictional shear effect between flow layers and weakened flow stability. Thus, the R_c increases.

Table 3 Initial velocity corresponding to different transport flow

Transport flow / m³/h	Pipe diameter / mm	Initial velocity m/s¹
180	200	1,592
200	200	1,769
220	200	1,946
240	200	2,123
260	200	2,300

Table 4 R_c under different experimental conditions

Slurry temperature / °C	Transport flow / m^3/h	R_c
30	180	164,45
40	180	187,24
50	180	212,79
60	180	242,68
30	200	199,20
40	200	226,61
50	200	257,19
60	200	292,82
30	220	236,57
40	220	268,89
50	220	304,81
60	220	346,46
30	240	276,43
40	240	313,93
50	240	355,45
60	240	403,38
30	260	318,64
40	260	361,58
50	260	408,92
60	260	463,37

3.2 Stowing Gradient Calculation

Three conditions for gravity transportation of UTBS can be obtained based on the comparison of N_{max} and N:

1) When $N_{max} > N$, the conveying outlet speed is greater than zero, and gravity transportation can be realized;

2) When $N_{max} = N$, the gravitational potential energy in the conveying process is completely used to overcome the resistance loss along the path. If the pumping mode is adopted, gravity transportation can be realized;

3) When $N_{max} < N$, gravity transportation can only be realized under external pressure, and the inlet velocity is not equal to the outlet velocity.

Tab. 5 shows the comparison between the set stowing gradient and the max allowable stowing gradient. Limited by space, the results are only shown for a slurry temperature of 40 °C, and other parameters are given in the same way.

Table 5 Comparison results of different stowing gradient

Transport flow / m^3/h	Slurry temperature / °C	Set stowing gradient	Max allowable stowing gradient
180	40	3	9,4
200	40	3	8,4
220	40	3	7,6
240	40	3	7,0
260	40	3	6,4
180	40	5	8,2
200	40	5	7,5
220	40	5	6,8
240	40	5	6,1
260	40	5	5,6
180	40	7	6,8
200	40	7	6,6
220	40	7	6,2
240	40	7	5,5
260	40	7	5,2

Tab. 5 indicates that the max allowable stowing gradient decreases with the increase of transport flow. Due to the increased transport flow, UTBS flow velocity increases, leading to an additional heat generated by friction between the pipe and the solid particles and consequently an increased resistance loss. Because the acceleration of gravity is constant for the same UTBS, resistance loss is inversely proportional with the stowing gradient.

When the stowing gradient is set to 3 and 5, it is less than the max allowable stowing gradient, therefore the gravity transportation can be realized. However, when the stowing gradient is set to 7, the max allowable stowing gradient is less than the set stowing gradient. Therefore, the UTBS can only be transported by external pressure. When the set stowing gradient is too large, the transport distance of UTBS is longer and the resistance loss is too large, resulting in the inability to transport by gravity, and it will increase the pipe wear, reduce the service time and raise the transport cost. However, when the setting stowing gradient is too small, the transport velocity will be larger, causing the transport stability to deteriorate and easily lead to pipeline burst. Based on the above analysis, the max stowing gradient is considered to be no more than 5 under experimental conditions in this paper.

3.3 Velocity Distribution of UTBS

Take the slurry temperature 30°C, stowing gradient 5 and transport flow 240 m^3/h (Fig. 5 and Fig. 6) as an example to explore the flow characteristics. The UTBS exhibits a structural flow in the vertical and horizontal pipe sections. After the junction between the bend and the horizontal pipe the velocity distribution changes. The reason is that the solid particles inside the UTBS are affected by gravity, and the ultrafine particles at the bottom of the pipe wall can form a lubricating layer that can promote the forward flow of the UTBS. When flowing from the bend into the horizontal pipe, the UTBS velocity direction changes. It would result in more intense particle collisions at the inner diameter of the pipe. Besides, the solid particles have a large friction with the pipe, which leads to the decrease of the inner diameter velocity. Finally, as shown in Fig. 5, the velocity field is gradually increasing from the bottom to the top of the pipe.

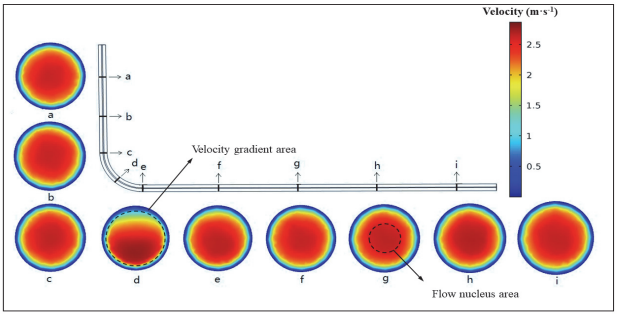

Figure 5 Flow velocity field of UTBS pipeline

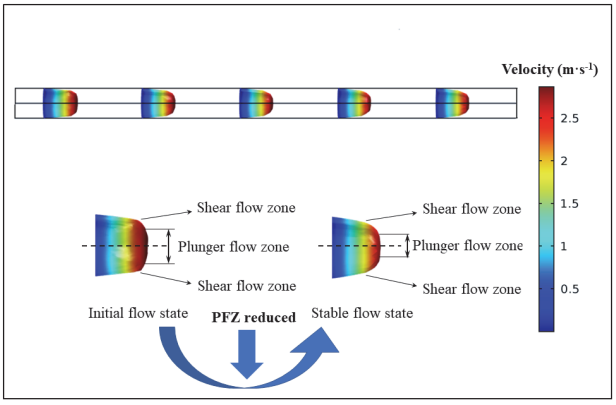

Figure 6 Velocity field vector variation of UTBS

The UTBS flows downward in a vertical pipe driven by gravity and creates mutual friction between each layer of slurry. The flow pattern is stabilized by the uniform gravitational force. In the transition zone between the bend and the horizontal pipe, gravity is no longer entirely responsible for the forward flow of the UTBS (see in Fig. 5 cross-sectional view d). After flowing into the horizontal pipe for a period of time, the velocity distribution of UTBS will slowly return to the form of structural flow, and there is a flow nucleus zone with the max velocity in the center. However, the change of slurry temperature has little effect on the change of convective state, and the flow is relatively stable with no turbulent zone, which is consistent with the judgment result of flow state.

Fig. 6 shows that the area of the flow core decreases gradually when the UTBS flows in the horizontal pipeline, indicating that the flow process of the horizontal pipeline will cause a high resistance loss. Consequently, the monitoring of the horizontal pipeline should be increased in the slurry transportation process to reduce the occurrence of pipe burst accidents caused by wear.

3.4 Influence Characteristics of Resistance Loss

3.4.1 Effect of Slurry Temperature

Fig. 7 indicates that the UTBS transport resistance loss decreases with the increase of slurry temperature. When the slurry temperature increases sequentially from 30 °C to 60 °C, the resistance loss decreases by 9% to 12%. In the horizontal pipe, the rheological parameters of the slurry change during pipeline transportation because of the increase in slurry temperature, which is manifested in the decreasing plastic viscosity and yield stress. This leads to a decreasing interaction between the solid particles and the frictional resistance between the flow layers of the UTBS. During the flow, the gravitational potential energy remains constant and the kinetic energy of slurry transport increases. Comparatively, friction losses, interaction forces and other "negative energy" are reduced, energy utilization is improved, and resistance loss is reduced. With the progress of slurry transportation, cement hydration reactions are constantly taking place and some hydration products are combined with the solid particles in UTBS. Under the wrapping effect of hydration products, the number of solid particles rubbing against the pipe wall is reduced, and the resistance loss is also decreased.

During the hydration reaction, the hydration product $Ca(OH)_2$ can further react with ultrafine SiO_2 particles to form the gel C-S-H. The specific process is as follows:

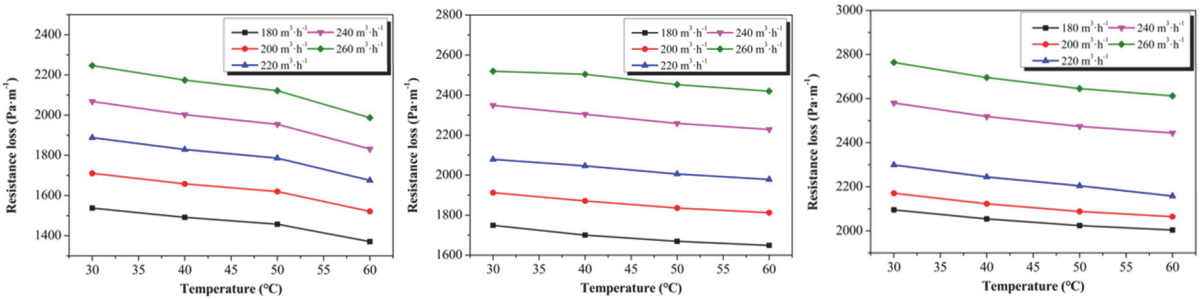

(a) Stowing gradient 3 (b) Stowing gradient 5 (c) Stowing gradient 7

Figure 7 Resistance loss curves of UTBS under different slurry temperatures

$$3CaO \cdot SiO_2 + nH_2O \rightarrow xCaO \cdot SiO_2 \left(n-3+x\right) H_2O + \left(3-x\right) Ca\left(OH\right)_2 \quad (10)$$

$Cao \cdot SiO_2 \cdot H_2O$ is called gel. The composition and structure of hydration products of ordinary silicate cement are usually influenced by the CaO and Al_2O_3 content in the fluid. In the tailings, SiO_2 is the main component and also includes a part of CaO and Al_2O_3. During slurry transportation, the C-S-H gel produced by the hydration reaction adsorbs the solid tailings particles and forms a flocculation structure, which then wraps the slurry to flow forward together. With the increase of slurry temperature, the rate of hydration reaction accelerates and the efficiency of gel generation combined with tailings particles increases, which reduces the number of solid particles in contact with the pipe wall in UTBS and leads to the reduction of resistance loss during transportation. In cement hydration process, there are usually four phases, including induction, stationary, acceleration and stabilization phases, of which only the induction and stationary phases have to be carried out for 2 h to fully react. Therefore, the hydration products continue to increase and the resistance loss keeps decreasing, indicating that the hydration reaction plays a positive role in reducing the transportation resistance.

3.4.2 Effect of Transport Flow

Fig. 8 shows that when the transport flow increases, the resistance loss of UTBS increases. In the process of UTBS transport, the ultrafine particles will form a lubricated flow layer at the bottom of the pipe, which has the effect of reducing the resistance loss. However, with the increase of the UTBS inlet flow, the initial velocity becomes increasingly larger. When UTBS flows from the bend into the horizontal pipe, the extrusion between the forward flowing particles increases, and many ultrafine particles cannot form the bottom lubrication layer in time. In this case, the frictional resistance between the UTBS solid phase particles and the pipe increases sharply, and the gravitational potential energy and kinetic energy of UTBS are used for frictional heat generation and loss, which eventually leads to an increase in the resistance loss during transportation.

When the stowing gradient is smaller, the increasing trend tends to be more linear. In Fig. 8a, there is a linear

increase relationship between the resistance loss and the transport flow of UTBS. In Fig. 8b and Fig. 8c, the trend of UTBS resistance loss changes when the transport flow is 220 m^3/h, and the trend grows with the increase of stowing gradient. The reason is that increasing the transport flow will not only increase the resistance loss during the transportation of UTBS, but also lead to an excessive inlet velocity. During pipeline transportation, the larger velocity can cause UTBS to impact the pipe wall excessively, leading to increased pipe wear and greatly shortening the service life of the pipe. Therefore, a reasonable flow for UTBS transportation need to be found. In this paper, it is suggested that the transport flow of 220 m^3/h is selected to reduce the pipeline wear, increase the service life of the pipeline, improve the conveying stability, and ensure the transport efficiency in the UTBS transportation.

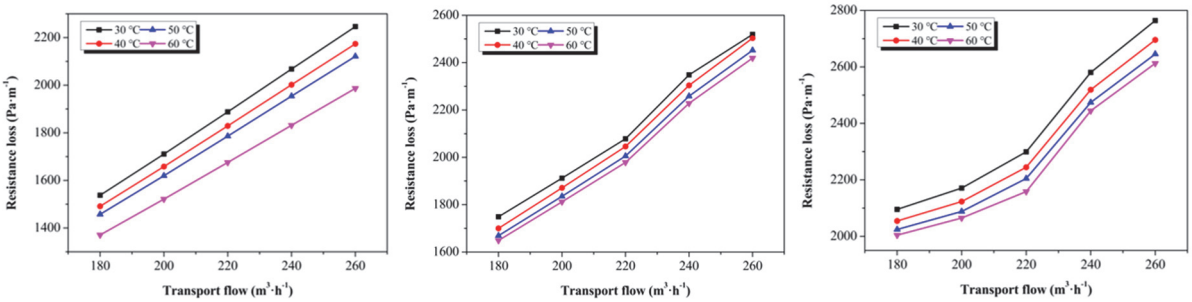

(a) Stowing gradient 3 (b) Stowing gradient 5 (c) Stowing gradient 7

Figure 8 Resistance loss curve of UTBS under different transport flow

3.4.3 Effect of Stowing Gradient

Fig. 9 indicates that the resistance loss of UTBS increases with the increase of stowing gradient. Under the same slurry temperature, the increasing trend of resistance loss at different transport flow is approximately the same when the stowing gradient increases from 3 to 5 and from 5 to 7.

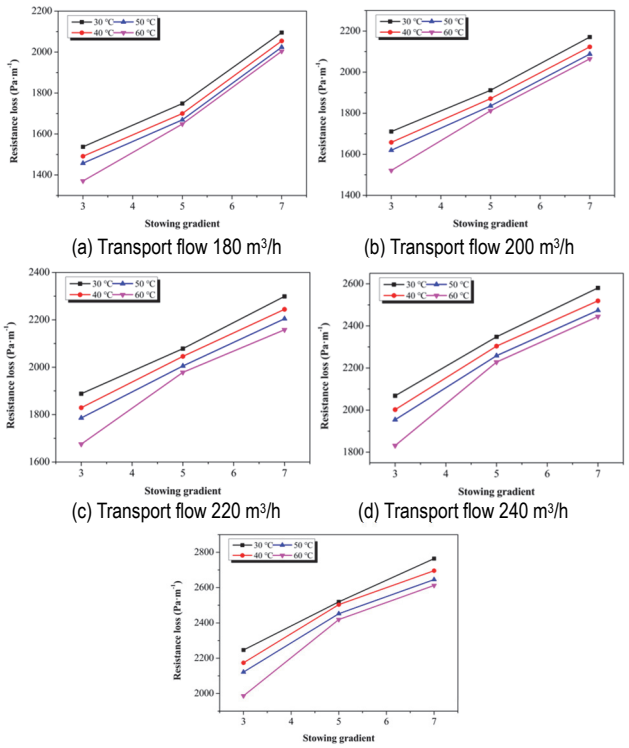

(a) Transport flow 180 m^3/h (b) Transport flow 200 m^3/h

(c) Transport flow 220 m^3/h (d) Transport flow 240 m^3/h

(e) Transport flow 260 m^3/h

Figure 9 Resistance loss curve of UTBS under different stowing gradient

When the stowing gradient increases from 3 to 7, the increasing trend of resistance loss is different for different transport flow. This means with the transport flow increases, the increasing trend gradually decreases, indicating that the effect of increasing stowing gradient on resistance loss starts to weaken when the transport flow increases. Eq. (6) shows that for the same UTBS, the stowing gradient is inversely proportional to the resistance loss. Therefore, the resistance loss becomes larger as the stowing gradient increases.

3.5 UTBS Pipeline Flow Transport Mechanism

Fig. 10 indicates that during UTBS transport, large-sized particles are subjected to their own gravity G and upward forces F (both buoyancy and inter-particle interaction forces). Differences in particle size lead to non-uniform interference settlement of solid particles during UTBS transportation [25, 26]. In this paper, the coarse particles would fall onto the "solution" formed by the fine solid particles and the UTBS transport carrier under the action of gravity, which causes the fine particles and the highly concentrated slurry solution to drive the coarse particles to flow forward together. The settling velocity and state of coarse particles themselves are affected and changed. With the increase of stowing gradient, the flow time of UTBS in horizontal pipe increases, which leads to the intensification of the phenomenon of "non-uniform interference settlement". A large number of relatively coarse particles would accumulate continuously in the middle and lower part of the pipe during the descent process to form. The fine particle size would be settled downward under the action of gravity and upward force first. Subsequently, the settling speed would be gradually reduced or even changed direction by the accumulated particles. The interaction between the particles increases, the heat generation of the flow process improves, and the resistance loss becomes larger.

Fig. 11 shows that during the UTBS transportation, the central zone advances with the structural flow with a constant velocity of diameter D_0 and velocity V_{st0}, and the shear flow zone near the sides of the pipe wall advances with velocity V_{sh0}. In the process of continuous flow, the particles in the UTBS have a migration law, which changes

the yield stress of the UTBS and causes the area of the structural flow zone and the shear flow zone to change to the central region advancing with the structural flow at a constant velocity of diameter D_1 and velocity V_{st1}, and the shear flow zone near both sides of the pipe wall at velocity V_{sh1}, which then affects the resistance loss [27]. In this paper, when the yield stress increases, the radial shear rate threshold increases in disguise. In Bingham plastic fluids, the constant velocity zone of the pipe gradually expands and the shear interaction zone between the slurry gradually reduces, which results in lower resistance loss. With the increase of the stowing gradient, there is no significant change in the trend of increasing velocity of UTBS in the horizontal pipe. However, the transport distance of UTBS in the pipe is continuously lengthened, the heat generated by the interparticle action in the pipe is increased, and the slurry temperature is rising. This leads to the lowering of the yield stress and the reduction of the area of the structural flow region in the pipe, which eventually makes the resistance loss of UTBS to increase.

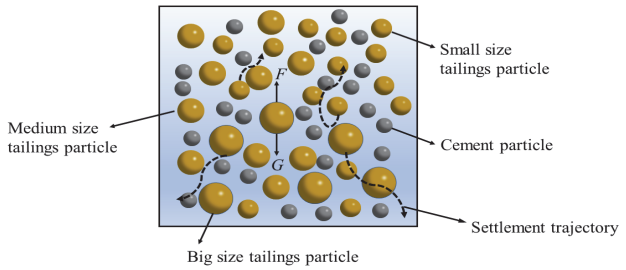

Figure 10 Solid particle interaction and settling process

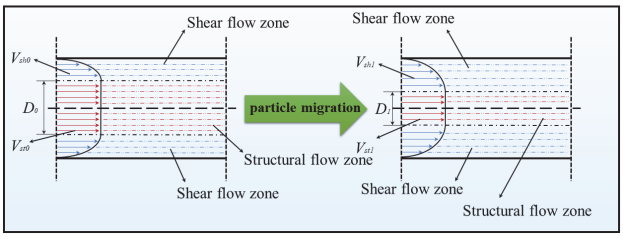

Figure 11 Flow area affected by coarse particle migration

4 CONCLUSIONS

(1) A new UTBS integrated Reynolds model considering the slurry temperature was proposed and applied to this simulation experiment data for flow evolution analysis.

(2) The velocity distribution of UTBS in the pipe was in the structural flow state, and the area of the flow core zone gradually decreased with the flow proceeded. When the slurry temperature increased sequentially from 30 ℃ to 60 ℃, the resistance loss decreased by 9% to 12%. It showed that the higher the slurry temperature, the greater the rate of resistance loss reduction.

(3) The transport mechanism of solid phase particles in the flow of UTBS was described. The particles with larger particle size were subject to settling action under the influence of gravity, traction and buoyancy. Because of the settling action leading to the accumulation of a large number of tailings particles in the lower part of the pipe, the settling tendency of the particles with smaller particle size in the flow process was weaker than the former. Therefore, the area of the structural flow zone decreased after the flow proceeded for a while. Meanwhile, a reason for the generation of resistance loss was also caused.

Considering the filling cost and transport efficiency, other mines could also select the suitable transport flow and stowing gradient based on the research results. In the future, with the improvement of mining efficiency, the high flow of cemented tailings backfill slurry transportation would become a development trend. Therefore, the results of this research would continue to provide a theoretical basis for mine pipeline transportation design.

Acknowledgments

This research was supported by the National Natural Science Foundation of China (Nos. 517704137, 51804121).

5 REFERENCES

[1] Li, M., Zhang, J. X., & Gao, R. (2015). A novel backfill material for roof supports in the cut-through entries of longwall mining. *Tehnicki Vjesnik*, *22*(1), 201-208. https://doi.org/10.17559/TV-20141130115523

[2] Kozior, T. (2020). Rheological Properties of Polyamide PA 2200 in SLS Technology. *Tehnicki Vjesnik*, *27*(4), 1192-1100. https://doi.org/10.17559/TV-20190225122204

[3] Yilmaz, E., Belem, T., Bussière, B., Mbonimpa, M., & Benzaazoua, M. (2015). Curing time effect on consolidation behaviour of cemented paste backfill containing different cement types and contents. *Construction and Building Materials*, *75*, 99-111. https://doi.org/10.1016/j.conbuildmat.2014.11.008

[4] Zhou, S. H., Li, X., Ji, C., & Xiao, J. (2017). Back-fill grout experimental test for discharged soils reuse of the large-diameter size slurry shield tunnel. *KSCE Journal of Civil Engineering*, 21(3), 725-733. https://doi.org/10.1007/s12205-016-0856-z

[5] Chen, L. Y., Duan, Y. F., Liu, M., &Zhao, C. S. (2010). Slip flow of coal water slurries in pipelines. *Fuel,89*(5), 1119-1126. https://doi.org/10.1016/j.fuel.2009.09.016

[6] Kaushal, D. R., Sato, K., Toyota, T., & Tomita, Y. (2005). Effect of particle size distribution on pressure drop and concentration profile in pipeline flow of highly concentrated slurry. *International Journal of Multiphase Flow*, *31*(7), 809-823. https://doi.org/10.1016/j.ijmultiphaseflow.2005.03.003

[7] Alireza, K. & Roohollah, Z. (2019). Statistical performance analysis of transient-based extended blockage detection in a water supply pipeline. *Journal of Water Supply: Research and Technology-AQUA*, *68*(5), 346-357. https://doi.org/10.2166/aqua.2019.014

[8] Byeon, H. & Park, J. (2023). Structural stability of stacked disposal containers in silo-type low- and intermediate-level waste repository under weight of backfilling materials. *Tunnelling and Underground Space Technology*, *133*, 104924. https://doi.org/10.1016/j.tust.2022.104924

[9] Celep, O. & Yazici, E. Y. (2017). Ultra fine grinding of silver plant tailings of refractory ore using vertical stirred media mill. *Transactions of Nonferrous Metals Society of China*, *23*(11), 3412-3420. https://doi.org/10.1016/S1003-6326(13)62882-4

[10] Kanta Das, S., Kundu, T., Dash, N., & Angadi, S. I. (2023). Separation behavior of Falcon concentrator for the recovery of ultrafine scheelite particles from the gold mine tailings. *Separation and Purification Technology*, *309*, 123065. https://doi.org/10.1016/j.seppur.2022.123065

[11] Xue, Z. L., Gan, D. Q., Zhang, Y. Z., & Liu, Z. Y. (2020). Rheological behavior of ultrafine-tailings cemented paste backfill in high-temperature mining conditions.

Construction and Building Materials, *253*, 119212. https://doi.org/10.1016/j.expthermflusci.2009.02.011
[12] Kasai, T. (1996). Effects of Temperature on Rheology of Fresh Cement Paste in High Flowing Concrete. *Journal of the Society of Materials Science Japan*, *45*(2), 230-234. https://doi.org/10.2472/jsms.45.230
[13] Deng, X., Klein, B., Tong, L., & Wit, D. B. (2018). Experimental study on the rheological behavior of ultra-fine cemented backfill. *Construction and Building Materials*, *158*(15), 985-994. https://doi.org/10.1016/j.conbuildmat.2017.05.085
[14] Petit, J. Y., Wirquin, E., & Khayat, K. H. (2010). Effect of temperature on the rheology of flowable mortars. *Cement and Concrete Composites*, *32*(1), 43-53. https://doi.org/10.1016/j.cemconcomp.2009.10.003
[15] Bras, A., Henriques, F. M. A., & Cidade, M. T. (2010). Effect of environmental temperature and fly ash addition in hydraulic lime grout behaviour. *Construction and Building Materials, 24*(8), 1511-1517. https://doi.org/10.1016/j.conbuildmat.2010.02.001
[16] Singh, K. P., Kumar, A., & Kaushal, D. R. (2019). Pressure drop calculation for fly ash slurry using rheological model. *Military operations research, 16*(6), 775-781. https://doi.org/10.1108/WJE-03-2019-0086
[17] Bartosik, A. (2016). Simulation of Reynolds number influence on heat exchange in turbulent flow of medium slurry. *Journal of Physics Conference*, *760*(1), 2-12. https://doi.org/10.1088/1742-6596/760/1/012002
[18] Meinhard, K. & Lackner, R (2008). Multi-phase hydration model for prediction of hydration-heat release of blended cements. *Cement and Concrete Research.*, *38*(6), 794-802. https://doi.org/10.1016/j.cemconres.2008.01.008
[19] Dilissen, N., Vleugels, J., Vermeiren, J., García-Baños, Marín José, J. R. S., & Catalá-Civera, M. (2023). Temperature dependency of the dielectric properties of hydrated and ordinary Portland cement and their constituent phases at 2.45 GHz up to 1100 °C. *Cement and Concrete Research*, *165*, 107067. https://doi.org/10.1016/j.cemconres.2022.107067
[20] Garres-Díaz, J., Fernández-Nieto, E. D., & Narbona-Reina, G. (2022). A semi-implicit approach for sediment transport models with gravitational effects. *Applied Mathematics and Computation*, *421*, 126938. https://doi.org/10.1016/j.amc.2022.126938
[21] Julyan, J. & Hutchinson, A. J. (2018). Conservation laws and conserved quantities of the governing equations for the laminar wake flow behind a small hump on a solid wall boundary. *International Journal of Non-Linear Mechanics*, *100*(4), 48-57. https://doi.org/10.1016/j.ijnonlinmec.2018.01.011
[22] Alaimo, G. & Zingales, M. (2015). Laminar flow through fractal porous materials: the fractional-order transport equation. *Communications in Nonlinear ence& Numerical Simulation*, *22*(1-3), 889-902. https://doi.org/10.1016/j.cnsns.2014.10.005
[23] Lyu, Z., Kenway, G. K., Paige, C., & Martins, J. (2013). Automatic Differentiation Adjoint of the Reynolds-Averaged Navier-Stokes Equations with a Turbulence Model. *Aiaa Computational Fluid Dynamics Conference*. https://doi.org/10.2514/6.2013-258
[24] Lee, S. J., Lee, J. H., & Kim, B. J. (2017). Improvement of the two-fluid momentum equation using a modified Reynolds stress model for horizontal turbulent bubbly flows. *Chemical Engineering Science*, *173*, 208-217. https://doi.org/10.1016/j.ces.2017.07.038
[25] Barnea, E. & Mednick, R. L. (1978). A Generalized approach to the fluid Dynamics of particulate systems part III: General correlation for the pressure drop through fixed beds of spherical particles. *The Chemical Engineering Journal*, *15*(3), 215-227. https://doi.org/10.1016/0300-9467(78)80006-9
[26] Li, S., Wang, X. M., & Zhang, Q. L. (2016). Dynamic experiments on flocculation and sedimentation of argillized ultrafine tailings using fly-ash-based magnetic coagulant. *Transactions of Nonferrous Metals Society of China*, *26*(7), 1975-1984. https://doi.org/10.1016/S1003-6326(16)64308-X
[27] Ovarlez, G., Bertrand, F., Coussot, P., & Chateau, X. (2012). Shear-induced sedimentation in yield stress fluids. *Journal of Non-Newtonian Fluid Mechanics*, *177-178*, 19-28. https://doi.org/10.1016/j.jnnfm.2012.03.013

Contact information:

Deqing GAN, Professor
College of Mining Engineering,
North China University of Science and Technology,
Tangshan, Hebei, China (063210)
E-mail: 743159060@qq.com

Haikuan SUN
(Corresponding author)
College of Mining Engineering,
North China University of Science and Technology
Tangshan, Hebei, China (063210)
E-mail: Sun159060@163.com

Yajie ZHANG
College of Mining Engineering,
North China University of Science and Technology
Tangshan, Hebei, China (063210
E-mail: Yajie187@163.com

Zhenlin XUE, Professor
College of Mining Engineering,
North China University of Science and Technology
Tangshan, Hebei, China (063210)
E-mail: 1470889608@qq.com